

GeoMask3D: Geometrically Informed Mask Selection for Self-Supervised Point Cloud Learning in 3D

Ali Bahri
ali.bahri.1@ens.etsmtl.ca

École de Technologie Supérieure,
Canada

Moslem Yazdanpanah
Moslem.Yazdanpanah.1@ens.etsmtl.ca

Mehrdad Noori
mehrdad.noori.1@ens.etsmtl.ca

Milad Cheraghalkhani
milad.cheraghalkhani.1@ens.etsmtl.ca

Gustavo Adolfo Vargas Hakim
gustavo-adolfo.vargas-hakim.1@ens.etsmtl.ca

David Osowiechi
david.osowiechi.1@ens.etsmtl.ca

Farzad Beizaei
farzad.beizaei.1@ens.etsmtl.ca

Ismail Ben Ayed
Ismail.BenAyed@etsmtl.ca

Christian Desrosiers
christian.desrosiers@etsmtl.ca

Abstract

We introduce a pioneering approach to self-supervised learning for point clouds, employing a geometrically informed mask selection strategy called GeoMask3D (GM3D) to boost the efficiency of Masked Auto Encoders (MAE). Unlike the conventional method of random masking, our technique utilizes a teacher-student model to focus on intricate areas within the data, guiding the model’s focus toward regions with higher geometric complexity. This strategy is grounded in the hypothesis that concentrating on harder patches yields a more robust feature representation, as evidenced by the improved performance on downstream tasks. Our method also presents a complete-to-partial feature-level knowledge distillation technique designed to guide the prediction of geometric complexity utilizing a comprehensive context from feature-level information. Extensive experiments confirm our method’s superiority over State-Of-The-Art (SOTA) baselines, demonstrating marked improvements in classification, and few-shot tasks.

1 Introduction

The advent of large-scale 3D datasets [8, 24] has propelled research on deep learning for point clouds, leading to notable improvements in complex 3D tasks. However, the time-consuming nature of data collection, compounded by the complexity of 3D view variations

and the mismatch between human perception and point cloud representation, significantly hinders the development of effective deep networks for this type of data [27]. In response to this challenge, Self-Supervised Learning (SSL) has emerged as a promising solution, facilitating the learning of representations without relying on manual annotations. SSL not only circumvents the issues of costly and error-prone labeling but also improves the model’s generalization ability, offering a pivotal advancement in the field of point cloud-based deep learning [6].

MAEs, as simple yet effective self-supervised learners, have gained prominence by learning to recover masked parts of data. This approach has significantly advanced NLP models and has resulted in exceptional vision-based representation learners [8, 11] when applied to vision tasks. Building on their success, MAEs have recently been adapted for point cloud representation learning, leading to SOTA methods including MaskPoint [14], Point-Bert [29], Point-MAE [16], Point-M2AE [30], I2P-MAE [31], and MAE3D [10]. Moreover, recent work on Masked Image Modeling (MIM) has shown the advantage of employing a targeted mask selection strategy [24]. This approach, based on the idea that focusing on more challenging regions enhances robust learning compared to reconstructing random masks, has obtained promising results for image processing. A primary reason for this strategy’s effectiveness is its ability to prioritize informative regions over background areas in images.

In this study, we explore how a targeted masking strategy can be applied to point cloud models within the MAE framework, applicable across both single and multi-scale methods. We introduce GeoMask3D (GM3D), a novel geometrically informed mask selection strategy for object point clouds. Due to the lack of background data in the object’s point clouds, GM3D enables models to concentrate on geometrically complex areas, such as canonical ones with higher connections to the other areas and paying less attention to the geometrically simple areas like smooth surfaces, as depicted in fig. 2. We refer solely to geometric characteristics as the input point cloud lacks color information (appearance features), and we only have access to a set of points across three axes (x , y , and z). To showcase the effectiveness of our method, we integrate it into the pretraining processes of both single-scale Point-MAE and multi-scale Point-M2AE, the leading MAE methods for point clouds. As illustrated in fig. 1, our method exhibits notable enhancements over the earlier SOTA approaches across a range of challenging tasks.

To the best of our knowledge, this represents the first attempt to implement a point-cloud-based masking strategy, independent of additional modalities such as multi-view images. Our contributions are summarized as follows:

1. We propose a novel masking strategy for point cloud MAEs, focusing on selecting

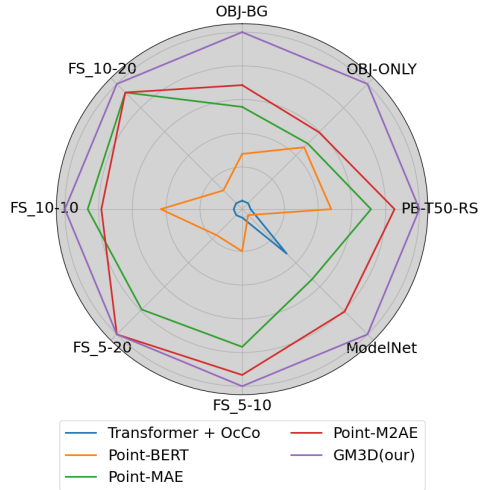


Figure 1: A relative comparison of the SOTA point cloud MAE methods on different tasks. Here, the center and the outer circles represent the lowest and highest values on each task, respectively.

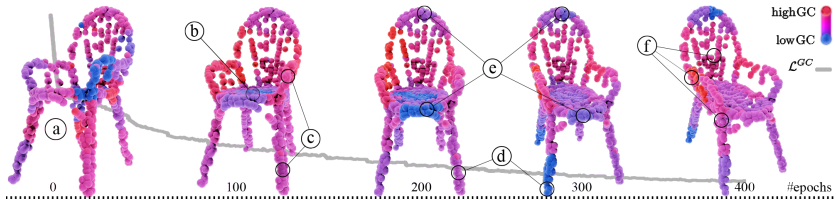


Figure 2: Visualization of estimated Geometric Complexity (GC) progression throughout training is depicted. The color spectrum denotes GC, ranging from low (Blue) to high (Red). GC values are normalized per object to reflect relative complexity across patches within each object’s point cloud. As training progresses (from left to right), initial GC rankings display a random distribution (a). After 100 epochs, the model learns to assign lower complexity rankings to smooth areas (b) and higher rankings to complex regions (c). Through GC guided masking, the model increasingly focuses on complex areas from epochs 200 to 300, resulting in a reduction of GC ranking (d) and smoothing of the complexity ranking distribution, accompanied by a decrease in total complexity loss \mathcal{L}^{GC} (e). Eventually, the model converges to a low \mathcal{L}^{GC} value, consistently targeting canonical patches while maintaining a smoother GC distribution (f).

geometrically complex patches rather than relying on random mask selection.

2. We present a complete-to-partial feature-level knowledge distillation technique that guides the geometric complexity prediction, utilizing a rich context from feature-level information.
3. We integrate these mechanisms into the pretraining process of single-scale Point-MAE and multi-scale PointM2AE, both of which are SOTA point cloud MAEs, achieving a considerable enhancement in their performance.

2 Related Works

Point Cloud Learning. PointNet [17], a pioneering point cloud-based learner, established point cloud processing as a key method in 3D geometric data analysis by addressing the permutation issue of point clouds with a max-pooling layer. To further enhance performance and enable the capture of both local and global features, PointNet++ [18] introduced a hierarchical structure, expanding the receptive fields of its kernels recursively for improved results over PointNet. Another study [9] focused on point cloud scene processing, where multi-view image features were combined with point clouds. In this study, 2D image features were aggregated into 3D point clouds, and a point-based network fused these features in 3D space for semantic labeling, demonstrating the substantial benefits of multi-view information in point cloud analysis. Furthermore, I2P-MAE [15] improved self-supervised point cloud processing by implementing a masking strategy, leveraging pre-trained 2D models through an Image-to-Point transformation.

MAE for Representation Learning. Leveraging the success of MAEs in Text and Image modalities, Point-BERT [19] introduced an approach inspired by BERT [4] adapting Transformers to 3D point clouds. This approach creates a Masked Point Modeling task, partitioning point clouds into patches and using a Tokenizer with a discrete Variational AutoEncoder (dVAE) to produce localized point tokens, with the goal of recovering original tokens at masked points. This BERT-style pretraining significantly improved point cloud Transformers, yielding higher accuracy across benchmarks. MaskPoint [14], a discriminative mask pretraining framework for point clouds, represents the point cloud with discrete

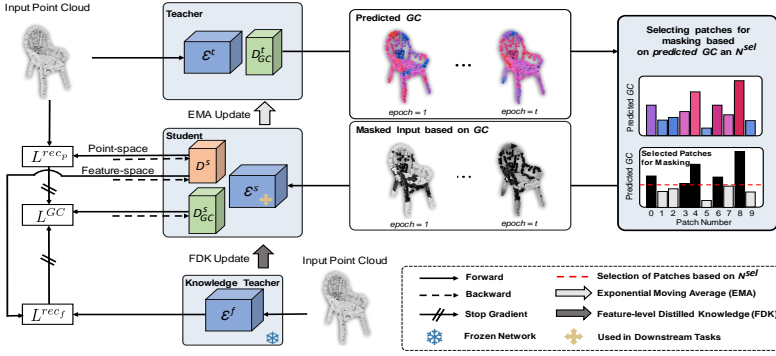


Figure 3: Overview of our GeoMask3D (GM3D) method for self-supervised representation learning in point clouds.

occupancy values and performs binary classification between object points and noise points, showing resilience to point sampling variance. Point-MAE [16] adapted MAE-style pre-training to 3D point clouds, employing a specialized Transformer-based autoencoder to reconstruct masked irregular patches and demonstrating strong generalization in various tasks. Following this, MAE3D [17] used a Patch Embedding Module for feature extraction from unmasked patches, while Point-M2AE [6] introduced a Multi-scale MAE framework with a pyramid architecture for self-supervised learning, focusing on fine-grained and high-level semantics. Point-M2AE’s multi-scale masking and local spatial self-attention mechanisms led to SOTA performance in 3D representation learning.

Our proposed method contrasts with these earlier approaches by offering a mask selection strategy that can be integrated into point cloud MAE methods, providing an alternative to the conventional random mask selection. Also, our study exclusively concentrates on pure point cloud processing methods, avoiding reliance on auxiliary information and 2D backbones as in recent point cloud learning methods like I2P-MAE [6].

3 Method

3.1 Preliminaries

Masked Auto Encoders. Autoencoders use an encoder \mathcal{E} to map an input X to a latent representation $Z = \mathcal{E}(X)$ and a decoder to reconstruct the input as $\hat{X} = \mathcal{D}(Z)$. Masked Auto Encoders (MAE) are a special type of autoencoder that receive a masked-patch input composed of a set of visible patches (with positional encoding) X^v and the index set of masked patches M , and reconstruct the masked patches as follows:

$$[X^v, \hat{X}^m] = \text{MAE}(X^v, M) = \mathcal{D}([\mathcal{E}(X^v), T_M]) \quad (1)$$

The encoder \mathcal{E} and decoder \mathcal{D} are both transformer-based networks. The encoder only transforms the visible patches to their latent representations $Z^v = \mathcal{E}(X^v)$. On the other hand, the decoder takes as input Z^v and a set of tokens $T_M = \{(t_{mask}, E_{pos}(i)) \mid i \in M\}$ where t_{mask} is a global learnable mask token and $E_{pos}(i)$ is the positional embedding of masked patch $i \in M$. Let $N = N^v + N^m$ be the number of patches in the input, with $N^v = |X^v|$ and $N^m = |M|$, the masking ratio is defined as $m^{ratio} = N^m/N$.

MAE for Point Clouds. A 3D point cloud P is a set of N^p points $p_j \in \mathbb{R}^3$. For this type of data, patches correspond to possibly overlapping subsets of K points in P . While there are various ways to generate patches from a point cloud, we follow the strategy employed by several related methods [14, 80] where each patch x_i is defined as a center point c_i and the set $P_i \subset P$ of K -Nearest Neighbours (KNN) to this center. To uniformly represent the whole point cloud, patch centers c_i are obtained using a Farthest Point Sampling (FPS) algorithm, where a first center is randomly chosen from P and then the next one is selected as the point in P furthest away from previously selected centers. Assuming that c_i is included as the first element of its nearest-neighbor list P_i , we can represent the patchified version of the point cloud as a tensor $X \in \mathbb{R}^{N \times K \times 3}$.

In autoencoders for images, a pixel-wise L2 reconstruction loss is typically used for training the MAE. In our case, since patches $x_i \in X$ are points sets, we instead employ the Chamfer distance to measure the reconstruction error \mathcal{L}^{rec_p} of masked patches:

$$\mathcal{L}^{rec_p} = \frac{1}{N^m} \sum_{i=1}^{N^m} \text{Chamfer}(x_i^m, \hat{x}_i^m), \quad (2)$$

where the Chamfer distance between two sets of points S and S' is defined as

$$\text{Chamfer}(S, S') = \sum_{p \in S} \min_{p' \in S'} \|p - p'\|_2^2 + \sum_{p' \in S'} \min_{p \in S} \|p - p'\|_2^2. \quad (3)$$

In the next section, we build on these definitions and present our GeoMask3D method for self-supervised point cloud representation learning.

3.2 GeoMask3D

We propose GeoMask3D (GM3D) as a modular component that integrates with any point cloud MAE backbone. This component is incorporated into the pretraining phase of a chosen method, shifting from a basic naive random masking approach to a selective focus on geometrically complex patches for masking. The architecture of GM3D employs an auxiliary head \mathcal{D}_{GC} for predicting the geometric complexity $GC \in \mathbb{R}^N$ across the input patches, which is trained with a loss \mathcal{L}^{GC} .

A teacher-student framework is utilized to integrate GM3D with a target network. We denote as $\text{GM3D}^s = (\mathcal{E}^s, \mathcal{D}^s, \mathcal{D}_{GC}^s)$ the student and $\text{GM3D}^t = (\mathcal{E}^t, \mathcal{D}^t, \mathcal{D}_{GC}^t)$ the teacher, both of them having their own encoder, decoder and auxiliary head. In line with [14], we apply a momentum update method to maintain a consistent teacher, updating it in each iteration,

$$\text{GM3D}^t = \mu \cdot \text{GM3D}^t + (1 - \mu) \cdot \text{GM3D}^s \quad (4)$$

where μ represents the momentum coefficient. Both networks predict the GC based on the patch’s informational content, as elaborated in section 3.2.1. We employ the prediction of GC in the masking strategy of the method during its pretraining stage. The GC of the student network (GC^s) is predicted based on the masked input X^v , while the GC of the teacher (GC^t) is calculated in inference mode using the complete input X :

$$GC^a = \begin{cases} \mathcal{D}_{GC}^a(\mathcal{E}(X)), & \text{if } a = t \text{ (teacher)} \\ \mathcal{D}_{GC}^a([\mathcal{E}(X^v), T_M]), & \text{if } a = s \text{ (student)} \end{cases} \quad (5)$$

The overview of our method for self-supervised representation learning in the point cloud is depicted in fig. 3. We further explain the mask selection strategy including its curriculum-based nature, in section 3.2.2 and section 3.2.3. This approach involves three interconnected steps:

3.2.1 Prediction of Geometric Complexity (GC)

During this stage, our goal is to evaluate GC of each patch in X^m , relative to the others within the same set. We achieve this by using a Dense Relation Comparison (DRC) loss [24] which enforces the GC of masked patch pairs (k, l) , predicted by the student (i.e., GC_k^s and GC_l^s), to follow the same relative order as their loss values $\mathcal{L}_k^{rec}, \mathcal{L}_l^{rec}$:

$$\mathcal{L}^{GC} = \sum_{k=1}^{N^m} \sum_{\substack{l=1 \\ l \neq k}}^{N^m} \mathcal{I}_{kl}^+ \log(\sigma(GC_k^s - GC_l^s)) - \mathcal{I}_{kl}^- \log(1 - \sigma(GC_k^s - GC_l^s)) \quad (6)$$

where $\mathcal{I}_{kl}^+ = \mathbb{1}(\mathcal{L}_k^{rec} > \mathcal{L}_l^{rec})$, $\mathcal{I}_{kl}^- = \mathbb{1}(\mathcal{L}_k^{rec} < \mathcal{L}_l^{rec})$, $\sigma(\cdot)$ is the sigmoid function, and \mathcal{L}^{rec} is detailed in section 3.3.

3.2.2 Geometric-Guided Masking

Patches with a high GC score are typically those that the model struggles to reconstruct accurately (see fig. 2). This difficulty often stems from their complex geometry, compounded by the absence of color and background information. While choosing those patches for masking might seem straightforward, there are two challenges to this approach. First, during training, the GC is evaluated by the student for masked patches X^m , yet we need to pick candidate patches from the entire set. Second, the student’s GC estimation can be noisy, making the training unstable. We address both these challenges by instead selecting patches based on the teacher’s score (GC^t). Thus, at each iteration, the teacher predicts the GC for all patches in X , including unmasked ones. Thanks to the momentum update of eq. (4), the teacher’s predictions are more consistent across different training iterations.

3.2.3 Curriculum Mask Selection

During the initial phases of training, the model may struggle to reconstruct fine details and is often overwhelmed by the complexity of the point cloud structure. To mitigate this problem, we follow a curriculum easy to hard mask selection strategy by starting from pure random masking at the initial training epoch and gradually increasing the portion of geometric-guided masking until the maximum epoch e_{max} . Let $A \in [0, 1]$ be the maximum ratio of patches that can be selected using GC^t . At each epoch e_t , we select the $N^{sel} = \lfloor e_t / e_{max} \times A \times N^m \rfloor$ patches with highest GC^t value, and the remaining $N^m - N^{sel}$ ones are selected randomly based on a uniform distribution.

3.3 Knowledge-Distillation-Guided GC

Instead of relying exclusively on point geometry, our approach employs a knowledge distillation strategy to also learn from latent features. This strategy involves transferring geometric knowledge from a frozen teacher network $F = (\mathcal{E}^f, \mathcal{D}^f)$ that processes the full set of patches to the student GM3D^s observing unmasked patches. This encourages the student GM3D^s to replicate the feature activations of the knowledge teacher F , indirectly learning from the full

structure of data. The complexity of patches in the feature space is determined by employing the Mean Square Error loss between the output of \mathcal{E}^f and the output of \mathcal{D}^s before converting back to point space:

$$\mathcal{L}^{rec_f} = \frac{1}{N^m} \sum_{i=1}^{N^m} \|\mathcal{E}^f(X)_i - \mathcal{D}^s([\mathcal{E}^s(X^v), T_M])_i\|^2 \quad (7)$$

This loss, combined with the Chamfer loss \mathcal{L}^{rec_p} applied in the point space, serves as the ground-truth loss \mathcal{L}^{rec} (8) for the prediction of GC. The final loss is observed in Equation (9).

$$\mathcal{L}^{rec} = \mathcal{L}^{rec_p} + \mathcal{L}^{rec_f} \quad (8) \quad \mathcal{L} = \alpha\mathcal{L}^{GC} + \beta\mathcal{L}^{rec_p} + \gamma\mathcal{L}^{rec_f} \quad (9)$$

4 Experiments

Several experiments are carried out to evaluate the proposed method. First, we pre-train both Point-MAE and Point-M2AE networks utilizing our GM3D approach on the ShapeNet [14] training dataset. Moreover, we assess the performance of these pre-trained models across a range of standard benchmarks, such as object classification, and few-shot learning. It is important to note that for downstream tasks, we exclusively utilize the encoder of the student network, ensuring it is identical to the encoder used in the method of interest, to maintain a completely fair comparison. In our approach, we adopt masking ratios with those used in the Point-MAE (60%) and Point-M2AE 80% models to guarantee a fully fair comparison. Additional visual experiments and our network’s hyperparameters are provided in the Supplementary Materials.

4.1 Pretraining Setup

Following Point-MAE and Point-M2AE, we adopt the ShapeNet dataset for the pre-training and we assess the quality of the 3D representations produced by our approach

through a linear evaluation on the ModelNet40 dataset [26]. The linear evaluation is performed by a Support Vector Machine (SVM) fitted on these features. This classification performance is quantified by the accuracy metrics detailed in Table 3.

4.2 Downstream Tasks

Object Classification on Real-World Dataset. In self-supervised learning for point clouds, we put our method to the test on the ScanObjectNN dataset [22], as detailed in previous works. We carry out tests on three different variants of this dataset: OBJ-BG, OBJ-ONLY,

Table 1: **Object classification on real-world ScanObjectNN dataset [22].** We evaluate our approach on three variants, among which PB-T50-RS is the hardest setting. Accuracy (%) for each variant is reported. \approx represents self-supervised pretraining.

Method	OBJ-BG	OBJ-ONLY	PB-T50-RS
PointNet [14]	73.3	79.2	68.0
SpiderCNN [25]	77.1	79.5	73.7
PointNet++ [14]	82.3	84.3	77.9
DGCNN [25]	82.8	86.2	78.1
PointCNN [14]	86.1	85.5	78.5
BGA-DGCNN [14]	-	-	79.7
BGA-PN++ [14]	-	-	80.2
GBNet [14]	-	-	80.5
PRANet [8]	-	-	81.0
Transformer [24]	79.86	80.55	77.24
\approx Transformer-OcCo [24]	84.85	85.54	78.79
\approx Point-BERT [24]	87.43	88.12	83.07
\approx Point-MAE [16]	90.02	88.29	85.18
\approx Point-MAE + GM3D	93.45	90.36	88.30
\approx Point-M2AE [16]	91.22	88.81	86.43
\approx Point-M2AE + GM3D	94.14	91.04	87.75

and PBT50-RS. The results of these experiments are reported in Table 1, demonstrating that the integration of GM3D with Point-MAE and Point-M2AE significantly boosts their object classification accuracy on this dataset. These findings underscore the strength of GM3D in boosting the models’ capacity to identify and classify objects against various backgrounds, proving its effectiveness in complex real-world scenarios.

Object Classification on Clean Objects Dataset. We evaluated our pre-trained models on the ModelNet40 dataset, as detailed in previous works. To ensure fair comparisons, the standard voting method [15] was also applied during the testing phase. According to table 3, integrating our GM3D module with Point-MAE yields classification accuracy of 94.20%, surpassing the performance of both the standalone Point-MAE and even Point-M2AE on the dataset. Given that our enhanced Point-MAE model has already achieved a higher accuracy than Point-M2AE, we did not proceed to test the GM3D module with Point-M2AE.

Few-shot Learning. Following the protocols of earlier studies [20, 23, 29], we conduct few-shot learning experiments on ModelNet40, using an n -way, m -shot configuration. Here, n is the number of classes randomly chosen from the dataset, and m is the count of objects randomly selected for each class. The $n \times m$ objects are utilized for training. During the test phase, we randomly sample 20 additional unseen objects from each of the n classes for evaluation. The results of our few-shot learning experiments are summarized in table 5. In this highly saturated benchmark, the combination of the GM3D module exhibits outstanding performance across all tested scenarios. It is worth noting that I2P-MAE [11] which *additionally benefits from multiple 2D views* provides only marginal improvements in results. Our findings highlight the effectiveness of our method as our Point-MAE+GM3D model has already achieved higher accuracy than single-scale Point-MAE and multi-scale Point-M2AE. Accordingly, we did not proceed to test the GM3D module with Point-M2AE.

4.3 Ablation Study

GM3D. Initially, we integrate the GM3D method with Point-MAE alongside \mathcal{L}^{recp} and \mathcal{L}^{GC} . As reported in table 4, this combination, termed Point-MAE+GM3D*, shows a clear improvement over the baseline model by achieving higher pretraining SVM and finetuning

Table 2: Ablation study on different maximum hard patch ratios (A).

Model	A	obj-only
Original Point-MAE	0	88.29
Point-MAE+GM3D	0.4	89.67
Point-MAE+GM3D	0.5	90.36
Point-MAE+GM3D	0.7	89.84

Table 3: **Linear evaluation on ModelNet40** [26]. ‘points’, ‘SVM’, and ‘Acc’ denote the number of points for training, training time validation accuracy of a support vector machine, and overall accuracy. \approx represents self-supervised pretraining.

Method	Points	Acc (%)	SVM
PointNet [16]	1k	89.2	-
PointNet++ [16]	1k	90.5	-
PointCNN [16]	1k	92.2	-
\approx SO-Net [16]	5k	92.5	-
DGCNN [16]	1k	92.9	-
PCT [6]	1k	93.2	-
Point Transformer [16]		93.7	-
Transformer [16]	1k	91.4	-
\approx Transformer + OcCo [16]	1k	92.1	89.6
\approx Point-BERT [16]	1k	93.2	-
\approx Point-BERT [16]	4k	93.4	-
\approx Point-BERT [16]	8k	93.8	87.4
\approx Point-M2AE [16]	1k	94.00	92.90
\approx Point-MAE [16]	1k	93.80	91.05
\approx Point-MAE + GM3D	1k	94.20	92.30

results on ScanObjectNN (OBJ-ONLY). This supports the idea that a training focus on more geometrically complex patches contributes to improved model generalization. Our ablation study focuses on the incremental improvements offered by our proposed method GM3D when integrated with the original Point-MAE framework using the Chamfer loss for self-supervised learning.

Building on this structure, we enhance the performance by incorporating knowledge distillation alongside the GM3D module. The improved model, Point-MAE+GM3D, which employs three distinct loss functions, not only outperforms the baseline Point-MAE but also shows further improvement over the Point-MAE+GM3D* approach that utilizes only \mathcal{L}^{recp} and \mathcal{L}^{GC} . This advancement validates the effectiveness of our knowledge distillation strategy. The various impacts of knowledge distillation are further explored in table 6.

Maximum Hard Patch Ratios. The data presented in table 2 offer insights into the ablation study focusing on different hardness ratios, denoted by A , within the context of point cloud modeling. It is noteworthy that the inclusion of GM3D enhances the performance across different A settings when compared to the original model, with the highest performance observed at a 50% hardness ratio, where the OBJ-ONLY score reaches 90.36%.

Additional Configurations. In table 6, which details our ablation study, investigating various configurations of our proposed method. As evidenced by the results, each setting has been systematically varied to assess its effect on the final performance metric, OBJ-ONLY, demonstrating the significant contributions of each component to the model’s learning efficacy. More details are provided in the Supplementary Materials.

5 Conclusion

We presented a geometrically-informed masked selection strategy for point cloud representation learning. Our GeoMask3D (GM3D) approach leverages a teacher-student model to find complex-to-reconstruct patches in the point cloud, which are more informative for learning robust representations. A knowledge distillation is further proposed to transfer rich geometric information from the teacher to the student, thereby improving the student’s reconstruc-

Table 4: Comparison of Point-MAE, and Point-MAE+GM3D on Pretraining (SVM) and Finetuning (OBJ-ONLY) Tasks. * Stands for Our Method without \mathcal{L}^{recf} .

Model	Loss Function	SVM	OBJ-ONLY
Point-MAE	\mathcal{L}^{recp}	91.05	88.29
Point-MAE+GM3D*	$\mathcal{L}^{recp}, \mathcal{L}^{GC}$	91.45	89.50
Point-MAE+GM3D	$\mathcal{L}^{recp}, \mathcal{L}^{recf}, \mathcal{L}^{GC}$	92.30	90.36

Table 5: **Few-shot classification on ModelNet40.** We report the average accuracy (%) and standard deviation (%) of 10 independent experiments. \approx represents self-supervised pertraining and in $A \approx$, A and std stand for average and standard deviation respectively.

Method	5-way		10-way	
	10-shot	20-shot	10-shot	20-shot
DGCNN [43]	91.8 \approx	93.4 \approx	86.3 \approx	90.9 \approx
\approx DGCNN + OcCo [43]	91.9 \approx	93.9 \approx	86.4 \approx	91.3 \approx
Transformer [44]	87.8 \approx	93.3 \approx	84.6 \approx	89.4 \approx
\approx Transf. + OcCo [44]	94.0 \approx	95.9 \approx	89.4 \approx	92.4 \approx
\approx Point-BERT [44]	94.6 \approx	96.3 \approx	91.0 \approx	92.7 \approx
\approx Point-M2AE	96.8 \approx	98.3 \approx	92.3 \approx	95.0 \approx
\approx Point-MAE	96.3 \approx	97.8 \approx	92.6 \approx	95.0 \approx
\approx Point-MAE + GM3D	97.0\approx	98.3\approx	93.1\approx	95.2\approx

Table 6: Ablation study on different components of our method based on Point-MAE

	Input $\rightarrow F$		\mathcal{L}		$\mathcal{L}^{rec} \rightarrow \mathcal{L}^{GC}$		$GM3D^f$	\mathcal{L}^{rec_f}	OBJ-ONLY
	X^v	X	\mathcal{L}^{rec_f}	\mathcal{L}^{rec_p}	\mathcal{L}^{rec_f}	\mathcal{L}^{rec_p}	μ		
<i>a</i>	✓		✓		✓		✓	$\mathcal{E}^f \rightarrow \mathcal{D}^s$	89.32
<i>b</i>	✓		✓	✓	✓	✓	✓	$\mathcal{E}^f \rightarrow \mathcal{D}^s$	90.18
<i>c</i>		✓	✓	✓		✓	✓	$\mathcal{E}^f \rightarrow \mathcal{D}^s$	89.67
<i>d</i>		✓		✓		✓	✓	$\mathcal{E}^f \rightarrow \mathcal{D}^s$	89.50
<i>e</i>		✓	✓	✓	✓	✓		$\mathcal{E}^f \rightarrow \mathcal{D}^s$	89.33
<i>f</i>		✓	✓	✓	✓	✓	✓	$\mathcal{E}^f \rightarrow \mathcal{E}^s$	89.15
<i>g</i>		✓	✓	✓	✓	✓	✓	$\mathcal{E}^f \rightarrow \mathcal{D}^s$	90.36

tion of masked point clouds. Comprehensive experiments on several datasets and downstream tasks show our method’s ability to boost the performance of point cloud learners. For future work, we aim to explore the application of our masking strategy, GM3D, across a broader range of SOTA methods, to further analyze and improve the mechanism of proposed geometrically informed mask selection.

References

- [1] Angel X Chang, Thomas Funkhouser, Leonidas Guibas, Pat Hanrahan, Qixing Huang, Zimo Li, Silvio Savarese, Manolis Savva, Shuran Song, Hao Su, et al. Shapenet: An information-rich 3d model repository. *arXiv preprint arXiv:1512.03012*, 2015.
- [2] Silin Cheng, Xiwu Chen, Xinwei He, Zhe Liu, and Xiang Bai. Pra-net: Point relation-aware network for 3d point cloud analysis. *IEEE Transactions on Image Processing*, 30:4436–4448, 2021.
- [3] Matt Deitke, Ruoshi Liu, Matthew Wallingford, Huong Ngo, Oscar Michel, Aditya Kusupati, Alan Fan, Christian Laforte, Vikram Voleti, Samir Yitzhak Gadre, et al. Objaverse-xl: A universe of 10m+ 3d objects. *arXiv preprint arXiv:2307.05663*, 2023.
- [4] Jacob Devlin, Ming-Wei Chang, Kenton Lee, and Kristina Toutanova. Bert: Pre-training of deep bidirectional transformers for language understanding. *arXiv preprint arXiv:1810.04805*, 2018.
- [5] Ben Fei, Weidong Yang, Liwen Liu, Tianyue Luo, Rui Zhang, Yixuan Li, and Ying He. Self-supervised learning for pre-training 3d point clouds: A survey. *arXiv preprint arXiv:2305.04691*, 2023.
- [6] Meng-Hao Guo, Jun-Xiong Cai, Zheng-Ning Liu, Tai-Jiang Mu, Ralph R Martin, and Shi-Min Hu. Pct: Point cloud transformer. *Computational Visual Media*, 7:187–199, 2021.
- [7] Kaiming He, Haoqi Fan, Yuxin Wu, Saining Xie, and Ross Girshick. Momentum contrast for unsupervised visual representation learning. In *Proceedings of the IEEE/CVF conference on computer vision and pattern recognition*, pages 9729–9738, 2020.

- [8] Kaiming He, Xinlei Chen, Saining Xie, Yanghao Li, Piotr Dollár, and Ross Girshick. Masked autoencoders are scalable vision learners. In *Proceedings of the IEEE/CVF conference on computer vision and pattern recognition*, pages 16000–16009, 2022.
- [9] Maximilian Jaritz, Jiayuan Gu, and Hao Su. Multi-view pointnet for 3d scene understanding. In *Proceedings of the IEEE/CVF International Conference on Computer Vision Workshops*, pages 0–0, 2019.
- [10] Jincen Jiang, Xuequan Lu, Lizhi Zhao, Richard Dazaley, and Meili Wang. Masked autoencoders in 3d point cloud representation learning. *IEEE Transactions on Multimedia*, 2023.
- [11] Jacob Devlin Ming-Wei Chang Kenton and Lee Kristina Toutanova. Bert: Pre-training of deep bidirectional transformers for language understanding. In *Proceedings of naacL-HLT*, volume 1, page 2, 2019.
- [12] Jiaxin Li, Ben M Chen, and Gim Hee Lee. So-net: Self-organizing network for point cloud analysis. In *Proceedings of the IEEE conference on computer vision and pattern recognition*, pages 9397–9406, 2018.
- [13] Yangyan Li, Rui Bu, Mingchao Sun, Wei Wu, Xinhan Di, and Baoquan Chen. Pointcnn: Convolution on x-transformed points. *Advances in neural information processing systems*, 31, 2018.
- [14] Haotian Liu, Mu Cai, and Yong Jae Lee. Masked discrimination for self-supervised learning on point clouds. In *European Conference on Computer Vision*, pages 657–675. Springer, 2022.
- [15] Yongcheng Liu, Bin Fan, Shiming Xiang, and Chunhong Pan. Relation-shape convolutional neural network for point cloud analysis. In *Proceedings of the IEEE/CVF conference on computer vision and pattern recognition*, pages 8895–8904, 2019.
- [16] Yatian Pang, Wenxiao Wang, Francis EH Tay, Wei Liu, Yonghong Tian, and Li Yuan. Masked autoencoders for point cloud self-supervised learning. In *European conference on computer vision*, pages 604–621. Springer, 2022.
- [17] Charles R Qi, Hao Su, Kaichun Mo, and Leonidas J Guibas. Pointnet: Deep learning on point sets for 3d classification and segmentation. In *Proceedings of the IEEE conference on computer vision and pattern recognition*, pages 652–660, 2017.
- [18] Charles Ruizhongtai Qi, Li Yi, Hao Su, and Leonidas J Guibas. Pointnet++: Deep hierarchical feature learning on point sets in a metric space. *Advances in neural information processing systems*, 30, 2017.
- [19] Shi Qiu, Saeed Anwar, and Nick Barnes. Geometric back-projection network for point cloud classification. *IEEE Transactions on Multimedia*, 24:1943–1955, 2021.
- [20] Charu Sharma and Manohar Kaul. Self-supervised few-shot learning on point clouds. *Advances in Neural Information Processing Systems*, 33:7212–7221, 2020.

- [21] Habib Slim, Xiang Li, Yuchen Li, Mahmoud Ahmed, Mohamed Ayman, Ujjwal Upadhyay, Ahmed Abdelreheem, Arpit Prajapati, Suhail Pothigara, Peter Wonka, and Mohamed Elhoseiny. 3DCoMPaT++: An improved large-scale 3d vision dataset for compositional recognition. 2023.
- [22] Mikaela Angelina Uy, Quang-Hieu Pham, Binh-Son Hua, Thanh Nguyen, and Sai-Kit Yeung. Revisiting point cloud classification: A new benchmark dataset and classification model on real-world data. In *Proceedings of the IEEE/CVF international conference on computer vision*, pages 1588–1597, 2019.
- [23] Hanchen Wang, Qi Liu, Xiangyu Yue, Joan Lasenby, and Matt J Kusner. Unsupervised point cloud pre-training via occlusion completion. In *Proceedings of the IEEE/CVF international conference on computer vision*, pages 9782–9792, 2021.
- [24] Haochen Wang, Kaiyou Song, Junsong Fan, Yuxi Wang, Jin Xie, and Zhaoxiang Zhang. Hard patches mining for masked image modeling. In *Proceedings of the IEEE/CVF Conference on Computer Vision and Pattern Recognition*, pages 10375–10385, 2023.
- [25] Yue Wang, Yongbin Sun, Ziwei Liu, Sanjay E Sarma, Michael M Bronstein, and Justin M Solomon. Dynamic graph cnn for learning on point clouds. *ACM Transactions on Graphics (tog)*, 38(5):1–12, 2019.
- [26] Zhirong Wu, Shuran Song, Aditya Khosla, Fisher Yu, Linguang Zhang, Xiaoou Tang, and Jianxiong Xiao. 3d shapenets: A deep representation for volumetric shapes. In *Proceedings of the IEEE conference on computer vision and pattern recognition*, pages 1912–1920, 2015.
- [27] Aoran Xiao, Jiaying Huang, Dayan Guan, Xiaoqin Zhang, Shijian Lu, and Ling Shao. Unsupervised point cloud representation learning with deep neural networks: A survey. *IEEE Transactions on Pattern Analysis and Machine Intelligence*, 2023.
- [28] Yifan Xu, Tianqi Fan, Mingye Xu, Long Zeng, and Yu Qiao. Spidercnn: Deep learning on point sets with parameterized convolutional filters. In *Proceedings of the European conference on computer vision (ECCV)*, pages 87–102, 2018.
- [29] Xumin Yu, Lulu Tang, Yongming Rao, Tiejun Huang, Jie Zhou, and Jiwen Lu. Pointbert: Pre-training 3d point cloud transformers with masked point modeling. In *Proceedings of the IEEE/CVF Conference on Computer Vision and Pattern Recognition*, pages 19313–19322, 2022.
- [30] Renrui Zhang, Ziyu Guo, Peng Gao, Rongyao Fang, Bin Zhao, Dong Wang, Yu Qiao, and Hongsheng Li. Point-m2ae: multi-scale masked autoencoders for hierarchical point cloud pre-training. *Advances in neural information processing systems*, 35: 27061–27074, 2022.
- [31] Renrui Zhang, Liuhui Wang, Yu Qiao, Peng Gao, and Hongsheng Li. Learning 3d representations from 2d pre-trained models via image-to-point masked autoencoders. In *Proceedings of the IEEE/CVF Conference on Computer Vision and Pattern Recognition*, pages 21769–21780, 2023.
- [32] Hengshuang Zhao, Li Jiang, Jiaya Jia, Philip HS Torr, and Vladlen Koltun. Point transformer. In *Proceedings of the IEEE/CVF international conference on computer vision*, pages 16259–16268, 2021.